Dalton Transactions

Accepted Manuscript

ROYAL SOCIETY OF CHEMISTRY

www.rsc.org/dalton

Journal Name

ARTICLE

Metallosupramolecular Ni_2L_3 and Ni_4L_6 complexes of bis-bidentate pyridine-containing ligands: X-ray structures and catalytic proton reduction

Received 00th January 20xx,
Accepted 00th January 20xx

DOI: 10.1039/x0xx00000x

www.rsc.org/

Chui-Shan Tsang, Lingjing Chen, Lu-Wei Li, Shek-Man Yiu, Tai-Chu Lau and Hoi-Lun Kwong*

The pyridine-containing ligands **L1** and **L2** react with Ni^{2+} ions to afford dinuclear triple-stranded helicate and tetrahedral cage supramolecular complexes, respectively; the two architectures exhibit contrasting reactivity towards electro- and photocatalytic proton reduction.

Introduction

The design and construction of metallosupramolecular complexes have been of great interest for more than two decades.[1–3] The coordination vector of the ligand strand is one of the important factors that govern the formation of various architectures,[4,5] and this has been well documented with monodentate ditopic or polytopic ligands.[6–8] It has also been shown that for these ligands any subtle variation of the ligand scaffold, including change in the binding motif and the bridging group between the binding domains, can lead to a change in the directional angle of the binding domains and the bend angle between them. In contrast, the effect of the directional angle of ligand's binding domains and the bend angle in bis-bidentate ditopic ligands on metallosupramolecular architectures is less clear.[3,9,10]

Reaction of bis-bidentate ditopic ligands with octahedral transition metal ions in a metal-to-ligand ratio of 2:3 usually affords polynuclear coordinatively saturated complexes,[3,9,10] but relatively few examples of Ni^{2+} metallosupramolecular architectures have been reported. Complexes of Ni^{2+} are of current interest as catalysts for electro- and photocatalytic H_2 evolution.[11] The use of earth abundant metals such as Ni as catalysts for the production of H_2 from water is a feasible strategy to cope with the increasing demand in energy and environmental pollution concern.[12] Inspired by recent examples of using polynuclear Ni^{2+} complexes as stable and efficient catalysts for electro- and photocatalytic H_2 evolution,[13,14] we herein describe the synthesis and structure of two novel metallosupramolecular architectures of Ni^{2+} based on the bis-bidentate ditopic ligands **L1** and **L2**, which possess different bridging groups, and their activities in electro- and photocatalytic H_2 evolution.

Department of Biology and Chemistry, City University of Hong Kong, Tat Chee Avenue, Kowloon, Hong Kong SAR (China) Fax: + 852 3442 0522; Tel: +852 3442 7304; E-mail: bhhoik@cityu.edu.hk

Electronic Supplementary Information (ESI) available: determinations of directional angle, crystallographic and structural data.

Experimental

General Procedure

Chemicals of reagent grade were obtained commercially. Chiral pyridinealdehyde **A** and chiral bidentate pyridyl-thiazole ligand **B** was prepared according to the reported procedures.[15,16] Chromatographic separations were performed with silica gel (60–200 μm; Merck) flash column chromatography. All ^1H, ^{13}C NMR, gCOSY spectra were recorded on a Varian 300 MHz Mercury instrument or a Bruker 400MHz instrument with tetramethylsilane (Sigma-Aldrich) as internal standard. Electron ionization mass spectra were recorded on a Hewlett Packard 5890II GC instrument coupled with a 5970 mass selective detector. Elemental analyses were performed on a Vario EL elemental analyzer. DLS measurements were performed on Zetasizer Nano ZS instrument (Malvern Instruments Ltd., USA), which can detect particle sizes ranging from 0.6–6000 nm. The light source of DLS was HeNe gas laser (4 mW, λ = 632.8 nm) and data were obtained by using scattering angle of 175° at 23 °C. SEM and EDX were performed by Philips XL30 environmental scanning electron microscope at accelerating voltage of 10 and 25 kV, respectively. Metal analysis was done on PE2100 ICP-AES.

X-ray crystallographic studies

Single crystals of $[Ni_2(\mathbf{L1})_3](ClO_4)_4$ and $[Ni_4(\mathbf{L2})_6](ClO_4)_8$ were obtained by slow diffusion of diethyl ether vapor into an acetonitrile solution and a mixture of MeOH–CH_2Cl_2 respectively. The X-ray structural data of $[Ni_2(\mathbf{L1})_3](ClO_4)_4$ and $[Ni_4(\mathbf{L2})_6](ClO_4)_8$ were collected by Oxford Diffraction CrystAlisPro at 293 K and 173 K respectively. The structures were solved by direct method with SHELX-97 by full matrix least-squares based on F^2. The non-hydrogen atoms were refined anisotropically while the hydrogen atoms were placed in idealized positions and assigned isotropic thermal parameters. In all cases, Friedel pairs were measured to

enable refinement of the Flack parameters which converged at 0.01(2) for $[Ni_2(\mathbf{L1})_3](ClO_4)_4$ and 0.02(1) for $[Ni_4(\mathbf{L2})_6](ClO_4)_8$ to confirm the absolute configurations. Details of the crystal parameters, data collection and refinement and selected metric parameters were summarized in supporting information Table S1–S3. Crystallographic data for the structures have been deposited to the Cambridge Crystallographic Data Centre as supplementary publication numbers CCDC 1059344 and 1059345.

Electrochemical studies

Cyclic voltammetry was performed on CHI 660C instrument and the electrochemical cell was of conventional design. A glassy carbon (3 mm diameter) was used as working electrode, a Pt wire as counter electrode and a non-aqueous $Ag/AgNO_3$ as reference electrode. All the electrochemical experiments were performed using 0.1 M TBHP in CH_3CN and the solution was purged with saturated argon or nitrogen. Ferrocene (Fc) was used as the internal standard, and all potentials are referenced to the ferrocenium/ferrocene ($Fc^{+/0}$) couple. All scans were done at 0.1 V/s. Trifluoroacetic acid (TFA, pK_a = 12.7 in CH_3CN) was used as proton source.

Photocatalytic H_2 evolution.

Photocatalytic H_2 evolution was conducted in a tube (1.8 cm × 18 cm, total volume of 28 mL) containing 2.5 mL acetone/H_2O (9:1, v/v) mixture. Samples typically contained 1 mM $[Ir(dF(CF_3)ppy)_2(dmbpy)]PF_6$ ($dF(CF_3)ppy$ = 2-(2,4-difluorophenyl)-5-trifluoromethylpyridine and dmbpy = 4,4′-dimethyl-2,2′-dipyridyl) as photosensitizer, 0.01–0.4 mM nickel catalyst and 0.2–0.6 M triethylamine (TEA, sacrificial reductant). The tube was sealed with a rubber septum. Argon saturated with acetone was then bubbled to the solution through a thin stainless syringe for 40 min at room temperature. The light source was a RGB tri-color LED light strip with 9 modules purchased from www.creativelightings.com. Each LED module consists of 3 light sources (blue, green and red) and the overall light colour is white (> 460 nm). The gas phase in the head space was analysed by GC/TCD (Galaxie 430) fitted with a Chrompack 5Å molecular sieve column (30 m × 0.32 mm ×1.5 μm) with argon as carrier gas. Calibration curve quantitatively analysis of H_2 are prepared by filling pure H_2 to a tube with a graduated gastight syringe.

Metal analysis.

The reaction solution after 26 h irradiation was transferred to a clean vial and the solvent was evaporated to dryness followed by addition of a mixture of conc. H_2SO_4–H_2O_2 (v/v = 1:1, 2 mL). The resulting solution was diluted with water to 10 mL and analysed by ICP-AES. The reaction flask and stirrer were also treated with the mixture of conc. H_2SO_4–H_2O_2 in the same way as the reaction solution, followed by the analysis using ICP-AES.

Synthesis of bis-pyridylimine ligand L1

Hydrazine monohydrate (0.055 g, 1.1 mmol) in ethanol (1 mL) was added dropwise into a stirring ethanolic solution (1 mL) of chiral pyridinealdehyde **A** (0.442 g, 2.2 mmol). The mixture was stirred at room temperature for 0.5 h. Suspension of pale yellow solids was observed afterwards and the reaction mixture was cooled in an ice-water bath for further precipitation. The solids were collected by filtration, washed with a cold solution mixture of ethanol–n-hexane (1:1, v:v) for three times and dried under vacuum: 0.023 g (54%); ^{1}H NMR (300 MHz, $CDCl_3$): 8.69 (s, 2H), 7.81 (d, 2H, *J* = 7.7 Hz), 7.51 (d, 2H, *J* = 7.6 Hz), 3.12 (t, 2H, *J* = 5.3 Hz), 2.99 (s, 4H), 2.65−2.83 (m, 2H), 2.25−2.42 (m, 2H), 1.43 (s, 6H), 1.31 (d, 2H, *J* = 9.9 Hz), 0.68 (s, 6H); ^{13}C NMR (100 MHz, $CDCl_3$): 21.27, 25.94, 30.72, 31.56, 39.11, 39.91, 50.30, 121.30, 132.77, 135.57, 148.57, 162.59, 166.89; ESI-MS: *m/z* 399.4 ($M + H^+$).

Synthesis of bromo-substituted ligand C

Chiral bidentate pyridyl-thiazole ligand **B** (5.77 g, 22.5 mmol) was dissolved in DMF (52 mL) with the suspension of Na_2CO_3 (2.7 g, 25.5 mmol). After the addition of Bromine (1.3 mL, 24.8 mmol), the resulting mixture was stirred at room temperature for 12 h. Saturated aqueous solution of Na_2SO_3 was added to quench the reaction. The organic layer was separated and the aqueous layer was extracted with diethyl ether for three times. The organic layer was collected and dried with $MgSO_4$. Solvent was removed under reduced pressure and crude brown oily product was afforded. Purification using flash column chromatography with petroleum ether (40–60 °C)/ethyl acetate (10:1) as eluent (R_f = 0.6). After removal of solvent, yellow oily product was afforded; pale yellow solid was then obtained on prolong standing: 4.53 g (60%); ^{1}H NMR (300 MHz, $CDCl_3$): 7.98 (s, 1H), 7.96 (d, 1H, *J* = 7.7 Hz), 7.53 (d, 1H, *J* = 7.9 Hz), 3.09 (t, 1H, *J* = 5.6 Hz), 2.99 (d, 2H, *J* = 2.4 Hz), 2.74–2.80 (m, 1H), 2.34–2.39 (m, 1H), 1.45 (s, 3H), 1.35 (d, 1H, *J* = 10.0 Hz), 0.71 (s, 3H); ^{13}C NMR (75 MHz, $CDCl_3$): 147.16, 141.51, 136.14, 132.42, 130.59, 117.43, 50.37, 40.23, 39.38, 31.68, 30.97, 26.16, 21.54; ESI-MS: *m/z* 304 ($M + H^+$).

Synthesis of bis-pyridylthiazole ligand L2

Bromo-substituted ligand **C** (10.1 g, 32 mmol), $Pd(PPh_3)_4$ (0.74 g, 0.64 mmol), hexa-n-butyltin (9.1 mL, 18.2 mmol) was dissolved in toluene, and heated at 110 °C with stirring for 12 h. The reaction mixture was cooled to room temperature, diluted with CH_2Cl_2 (50 mL) and extracted with brine for three times. The organic layer was collected and dried with $MgSO_4$, and the solvent was removed under reduced pressure to afford crude brown oily product. The crude product was recrystallized in hot methanol. The resulting bright yellow solids were collected by filtration and dried under vacuum: 3.9 g (48%); ^{1}H NMR (300 MHz, $CDCl_3$): 7.98 (s, 2H), 7.96 (d, 2H, *J* = 7.7 Hz), 7.53 (d, 2H, *J* = 7.9 Hz), 3.09 (t, 2H, *J* = 5.6 Hz), 2.99 (d, 4H, *J* = 2.4 Hz), 2.74–2.80 (m, 2H), 2.34–2.39 (m, 2H), 1.45 (s, 6H), 1.35 (d, 2H, *J* = 10.0 Hz), 0.71 (s, 6H); ^{13}C NMR (75 MHz, $CDCl_3$): 169.50, 166.84, 147.16, 141.51, 136.14, 132.42, 130.59, 117.43, 50.37, 40.23, 39.38, 31.68, 30.97, 26.16, 21.54. ESI-MS: *m/z* 511 ($M + H^+$).

Synthesis of $[Ni_2(L1)_3](ClO_4)_4$

$Ni(ClO_4)_2{\cdot}6H_2O$ (0.016 g, 0.04 mmol) was dissolved in acetonitrile (2 mL), followed with the addition of **L1** (0.023 g, 0.06 mmol). The resulting pale yellow solution was stirred at room temperature for 3 h, and pale brown crystals were afforded under slow diffusion with diethyl ether vapor. The crystals were filtered, collected and dried under vacuum: 0.053 g (78%); ESI-MS: *m/z* 954.1 $[Ni(C_{26}H_{30}N_4)_2(ClO_4)]^+$, 1612.0 $[Ni_2(C_{26}H_{30}N_4)_3(ClO_4)_3]^+$; CHN

elemental analysis calc. for $Ni_2(C_{26}H_{30}N_4)_3(ClO_4)_4 \cdot 12H_2O$: C, 48.62; H, 5.96; N, 8.72; found: C, 48.89; H, 5.90; N, 8.26.

Synthesis of $[Ni_4(L2)_6](ClO_4)_8$

$Ni(ClO_4)_2 \cdot 6H_2O$ (0.037 g, 0.1 mmol) was dissolved in the mixture of CH_3OH–CH_2Cl_2 (1:1) (5 mL), followed with the addition of **L2** (0.077 g, 0.15 mmol). The resulting yellowish green solution was stirred at room temperature for 4 h, followed by precipitation with diethyl ether to afford yellowish green crude solids. It was filtered, collected and dried under vacuum: 0.085 g (83%); ESI-MS: *m/z* 667.5 $[Ni(C_{30}H_{30}N_4S_2)(ClO_4)]^+$, 1948.6 $[Ni_4(C_{30}H_{30}N_4S_2)_6(ClO_4)_6]^{2+}$; CHN elemental analysis calc. for $Ni_4(C_{180}H_{180}N_{24}S_{12})(ClO_4)_8 \cdot 2CH_2Cl_2 \cdot 2CH_3OH$: C, 51.04; H, 4.48; N, 7.77; found: C, 51.25; H, 4.51; N, 7.48.

Results and discussion

Synthesis and characterizations

Pale yellow solids of ligand **L1** were afforded by the condensation of chiral pyridinealdehyde **A**[15] and hydrazine monohydrate in a ratio of 2:1 with the yield of 54% (Scheme 1). The solids were pure enough for complexation without recrystallization. For ligand **L2**, with the bromination of chiral bidentate pyridyl-thiazole ligand **B**,[16] followed by palladium-catalyzed homocoupling of **C**, crude brown solids were afforded (Scheme 2). The crude solids of **L2** were recrystallized in hot methanol, and bright yellow solids were obtained afterwards in 45% yield. Characterization of the pure solids of both **L1** and **L2** with NMR spectroscopy and ESI-MS indicated their successful synthesis.

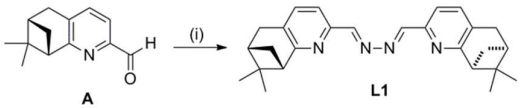

Scheme 1. Synthesis of bis-pyridylimine ligand **L1**. Reagents and conditions: (i) $N_2H_4 \cdot H_2O$, ethanol, rm. temp.

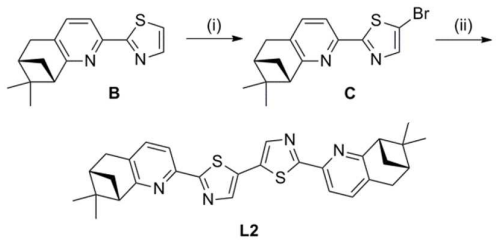

Scheme 2. Synthesis of bis-pyridylthiazole ligand **L2**. Reagents and conditions: (i) Br_2, Na_2CO_3, rm. temp.; (ii) $Pd(PPh_3)_4$, $(SnBu_3)_2$, toluene, 100 °C, 12 h.

Reaction of $Ni(ClO_4)_2$ with **L1** in CH_3CN and **L2** in a mixture of CH_2Cl_2–CH_3OH, both in a metal-to-ligand ratio of 2:3, afforded crude pale brown and yellowish green solids, respectively, after precipitation with diethyl ether. Elemental analysis of the two crude solids showed identical metal-to-ligand ratio of 2:3, but the ESI-MS spectra review that they have different structures. The MS of the Ni–**L1** product exhibits a monocationic peak at *m/z* 1612.0 corresponding to $[Ni_2(L1)_3(ClO_4)_3]^+$, suggesting that its formula is $[Ni_2(L1)_3](ClO_4)_4$, with a possible dinuclear triple-stranded helical structure. On the other hand, a dicationic peak at *m/z* 1948.6 corresponding to $[Ni_4(L2)_6(ClO_4)_6]^{2+}$ is observed for the Ni–**L2** product, suggesting that it is probably a tetrahedral cage of formula $[Ni_4(L2)_6](ClO_4)_8$. As the circular dichroism (CD) spectra of both $[Ni_2(L1)_3]^{4+}$ and $[Ni_4(L2)_6]^{8+}$ are identical before and after recrystallization, we believe the formations of both $[Ni_2(L1)_3]^{4+}$ and $[Ni_4(L2)_6]^{8+}$ are stereoselective.

X-ray crystallographic studies

The proposed structures of the Ni complexes were confirmed by X-ray crystallographic studies of their single crystals. In the structure of $[Ni_2(L1)_3](ClO_4)_4$, three ligand strands of **L1** are wrapped around two Ni ions, resulting in a triple helical structure of *M*-configuration (Figure 1). Each Ni ion is facially coordinated by three bidentate pyridyl-imine binding domains of each ligand strand in a distorted octahedral geometry and is Λ-configured. Helical twist arises at the interannular N–N bond of the ligand strand between the binding domains. Comparing with the reported dinuclear Ni(II) triple-stranded helicate of an achiral bis-pyridylimine ligand,[17] larger helical twist (94°) and longer Ni···Ni distance (3.8331 Å) and Ni–N distances (2.089–2.213 Å) are observed in $[Ni_2(L1)_3](ClO_4)_4$.

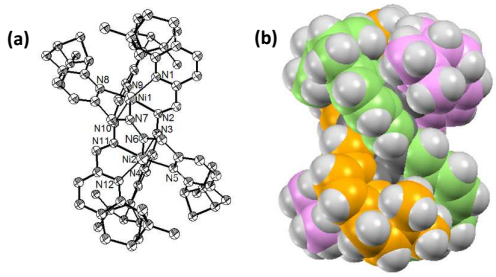

Figure 1. (a) OPTEP plot of $[Ni_2(L1)_3]^{4+}$ with partial atoms labelling. H atoms are removed for clarity. (b)Space-filling model of $[Ni_2(L1)_3]^{4+}$ with coloured ligand strand emphasizes the helical structure.

The structure of $[Ni_4(L2)_6](ClO_4)_8$ shows that Ni and **L2** act as the vertices and edges, respectively, of a tetrahedral cage (Figure 2). The Ni···Ni separations are in the range of 9.736–9.796 Å. Each Ni is facially coordinated with three bidentate pyridyl-thiazole binding domains from three ligand strands in a distorted octahedral geometry with Λ configuration. The Ni–N distances at pyridine (2.176–2.205 Å) are slightly longer than that at thiazole (2.067–2.102 Å), and these distances are comparable with the Ni^{2+} complex of a pyridylthiazole ligand reported in the literature.[18] Twisting between the bidentate binding domains of **L2** is observed in the six edges of the Ni_4 cage, and the twisting angle is 111.24° in three of them and 118.85° for the others.

Analysis of the X-ray structures of $[Ni_2(L1)_3](ClO_4)_4$ and $[Ni_4(L2)_6](ClO_4)_8$ reviews the difference in the directional angle of binding domains of **L1** and **L2**. In **L1**, the directional angle of the bidentate pyridyl-imine binding domains defined by the angle between the resultant coordination vector of the Ni–N coordination vectors and the interannular N–N bond between the binding domains is found to be 84.5° (Figure S1). In comparison, in **L2**, a larger directional angle of 110.5° is found for the bidentate pyridyl-thiazole binding domains defined by the angle between the resultant coordination vector of the Ni–N coordination vectors and the interannular C–C bond between the binding domains (Figure

S2). The analysis shows that the bridging group affects the directional angle of ligand's binding domains, resulting in the formation of different metallosupramolecular architectures.

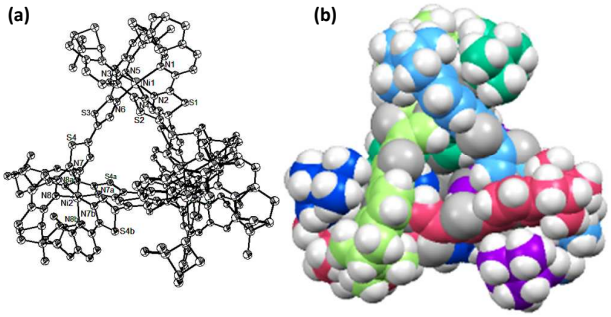

Figure 2. (a) OPTEP plot of $[Ni_4(\mathbf{L2})_6]^{8+}$ with partial atoms labelling. H atoms are removed for clarity. (b)Space-filling model of $[Ni_4(\mathbf{L2})_6]^{8+}$ with coloured ligand strands.

Electrocatalytic activity in proton reduction

The electrocatalytic activity of the Ni_2 helicate and the Ni_4 cage in proton reduction was investigated by cyclic voltammetry (CV). The CV of $[Ni_2(\mathbf{L1})_3](ClO_4)_4$ in CH_3CN shows two reduction waves at −0.47 V and −0.99 V *vs* $Fc^{+/0}$, which are assigned to the successive reduction of two Ni centers from Ni^{2+} to Ni^{+}, while the reduction wave at −2.01 V is assigned to the further reduction of a Ni^{+} to Ni^{0} (Figure S3a). The small reduction waves observed at –0.73 V and –1.27 V may be due to minor degradation of the helicate. No catalytic wave was observed upon the addition of trifluoroacetic acid (TFA) to the Ni_2 helicate (Figure S3b), indicating that $[Ni_2(\mathbf{L1})_3]^{4+}$ is an inactive proton reduction catalyst. On the other hand, $[Ni_4(\mathbf{L2})_6](ClO_4)_8$ readily catalyses proton reduction. The CV of the Ni_4 cage shows two broad reduction waves at −1.36 V and −1.46 V, which are assigned to the successive reduction of two Ni^{2+} centres to Ni^{+}. There are also another set of broad waves at −2.12 V and −2.22 V, which are assigned to the reduction of the ligand and the remaining two Ni^{2+} centres to Ni^{+} (Figure S4). Addition of TFA triggered a catalytic wave at a potential (ca. −1.35 V) close to the $Ni^{II}_4/Ni^{II}_3Ni^{I}$ couple, and the catalytic current increased with increasing TFA, consistent with the occurrence of catalytic proton reduction.[19] The overpotential was determined to be approximately 430 mV using the method of Evans et al (Figure 3).[20] The apparent maximum current intensity of the catalytic waves displays a linear dependence on the concentration of TFA (Figure 3), indicating a second-order dependence of the reaction rate on acid concentration.[21] These results indicate that the Ni_4 cage is active in electrocatalytic proton reduction while the Ni_2 helicate is not, presumably because the $Ni^{II/I}$ redox potentials of Ni_2 helicate are less negative than the Ni_4 cage.

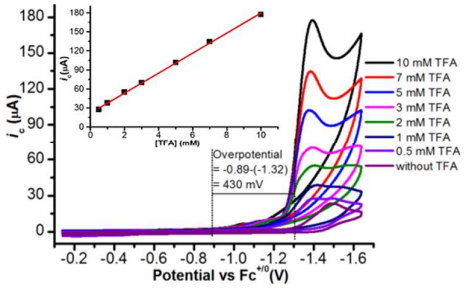

Figure 3. Cyclic voltammograms of 0.25 mM $[Ni_4(\mathbf{L2})_6](ClO_4)_8$ in the absence and presence of TFA. The insert shows the plot of i_c versus the concentration of TFA.

Photocatalyic activity in proton reduction

The photocatalytic activity of the Ni_2 helicate and the Ni_4 cage towards proton reduction was evaluated by using $[Ir(dF(CF_3)ppy)_2(dmbpy)]PF_6$ as the photosensitizer (PS) and triethylamine (TEA) as the sacrificial reductant, with a white LED light of λ > 460 nm. Control experiments showed that no H_2 was detected in the absence of the PS or the sacrificial reductant. The Ni_4 cage was found to be an active photocatalyst for proton reduction, and the performance of the catalyst depends on the concentration of the catalyst and the sacrificial reductant. Under the optimum conditions using of Ni_4 cage and 0.6 M TEA in a mixture of acetone–water (9:1, v/v), turnover numbers (TONs) of 2509 and 4623 were obtained after 8 h and 26 h irradiation, respectively (Figure 4). On the other hand, even though various conditions had been tried, the Ni_2 helicate showed no activity in photocatalytic proton reduction.

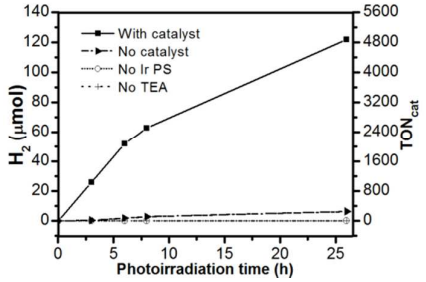

Figure 4. Photocatalytic proton reduction from 0.01 mM $[Ni_4(\mathbf{L2})_6](ClO_4)_8$, 1 mM PS, 0.6 M TEA;

In catalytic proton reduction a molecular metal complex may function only as a precatalyst which may decompose under the reaction conditions to the metal which is the real catalyst.[11,22] To investigate whether the photocatalysis by $[Ni_4(\mathbf{L2})_6](ClO_4)_8$ is homogeneous or heterogeneous in nature, mercury poisoning experiment was performed. The result shows that the total amount of H_2 is reduced by 77% compared with that in the absence of Hg(0) after 26 h irradiation (Figure 5). This suggests that the system is heterogeneous in nature, and the Ni complex is decomposed to Ni particles during photocatalytic hydrogen evolution, which are possibly the real catalytic species.[22] Recently, Ni(0) nanoparticles have been used in photocatalytic hydrogen evolution with high efficiency, and one of the possible ways for its formation is to use a nickel(II) complex as precursor.[11,23,24] Although no nanoparticles

could be detected in the Ni_4 reaction solution by dynamic light scattering (DLS), black coatings were observed on the surface of the stirrer and the flask after irradiation. Analysis of the Ni content in the reaction solution and the black coating (after dissolution in acid) after irradiation by inductively coupled plasma atomic emission spectroscopy (ICP-AES) indicated that 23% of Ni was found in the reaction solution while the remaining 77% of Ni was found in the black coatings on the wall of the flask and the stirrer.

The photocatalytic proton reduction study shows that the Ni_4 cage functions as precatalyst and undergoes in situ transformation to the catalytically active Ni(0) species during photocatalytic proton reduction. Although the Ni_2 helicate was decomposed as well, the contrasting reactivity of the Ni_2 helicate and the Ni_4 cage suggests that the bridging group modification on ligand strands influences, not only the formation of metallosupramolecular architectures and the lability of the ligands, but also the formation of active catalytic species during catalysis. As the Ni_4 catalyst is more efficient than simple Ni(II) salts such as $Ni(ClO_4)_2$ (Figure 5), this result suggests that ligand probably plays an important role in the formation or even affecting the structure of the catalytically active species.

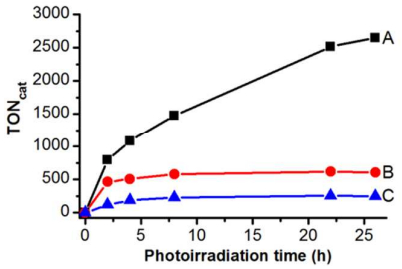

Figure 5. Photocatalytic proton reduction of (**A**) 0.04 mM $[Ni_4(\mathbf{L2})_6](ClO_4)_8$; (**B**) 0.04 mM $[Ni_4(\mathbf{L2})_6](ClO_4)_8$ + 0.5 mL Hg(0); (**C**) 0.16 mM $Ni(ClO_4)_2$.

Conclusions

We have demonstrated that variation of the bridging group between the binding domains of ligand strands affects the directional angle, resulting in Ni(II) complexes of different architectures, namely triple-stranded helicate $[Ni_2(\mathbf{L1})_6](ClO_4)_8$ and tetrahedral cage $[Ni_4(\mathbf{L2})_6](ClO_4)_8$. The Ni_4 cage is an active catalyst for electro- and photocatalytic proton reduction but the Ni_2 helicate is not, presumably because the $Ni^{II/I}$ redox potentials of Ni_4 complex occur at more negative potentials than the Ni_2 complex. These results indicate that bridging group modification on the ligand strands influences not only the metallosupramolecular architectures but also the redox potentials and hence the catalytic activities. To the best of our knowledge, this is the first example of using $M_4\mathbf{L}_6$ tetrahedral cage as catalyst for electro- and photocatalytic proton reduction. Further studies are ongoing to identify the nature of the real catalytic species of the Ni_4 cage system in order to have a better understanding on the mechanism of both electro- and photocatalytic proton reduction. In addition, ligand effect on the activity of the catalytic species will be also studied to further improve the activity.

Acknowledgements

This work was supported by the Hong Kong University Grants Committee Area of Excellence Scheme (AoE/P-03-08) and the City University of Hong Kong (SRG 7004208).

Notes and references

1. R. Chakrabarty, P. S. Mukherjee and P. J. Stang, *Chem. Rev.*, 2011, **111**, 6810.
2. T. K. Ronson, S. Zarra, S. P. Black and J. R. Nitschke, *Chem. Commun.*, 2013, **49**, 2476.
3. M. D. Ward and P. R. Raithby, *Chem. Soc. Rev.*, 2013, **42**, 1619.
4. D. L. Caulder and K. N. Raymond, *Acc. Chem. Res.*, 1999, **32**, 975.
5. N. J. Young and B. P. Hay, *Chem. Commun.*, 2013, **49**, 1354.
6. D. Fiedler, D. H. Leung, R. G. Bergman and K. N. Raymond, *Acc. Chem. Res.*, 2005, **38**, 349.
7. Q.-F. Sun, J. Iwasa, D. Ogawa, Y. Ishido, S. Sato, T. Ozeki, Y. Sei, K. Yamaguchi and M. Fujita, *Science*, 2010, **328**, 1144.
8. J. Bunzen, J. Iwasa, P. Bonakdarzadeh, E. Numata, K. Rissanen, S. Sato and M. Fujita, *Angew. Chem. Int. Ed.*, 2012, **51**, 3161.
9. M. D. Ward, *Chem. Commun.*, 2009, 4487.
10. M. M. J. Smulders, I. A. Riddell, C. Browne and J. R. Nitschke, *Chem. Soc. Rev.*, 2013, **42**, 1728.
11. (a) L. Chen, G. Chen, C.-F. Leung, S.-M. Yiu, C.-C. Ko, E. Anxolabéhère-Mallart, M. Robert and T.-C. Lau, *ACS Catal.*, 2015, **5**, 356. (b) A. Das, Z. Han, W. W. Brennessel, P. L. Holland and R. Eisenberg, *ACS Catal.*, 2015, **5**, 1397. (c) L. Gan, T. L. Groy, P. Tarakeshwar, S. K. S. Mazinani, J. Shearer, V. Mujica and A. K. Jones, *J. Am. Chem. Soc.*, 2015, **137**, 1109 and references therein.
12. G. Zini and P. Tartarini, *Solar Hydrogen Energy Systems*, Springer-Verlag Mailand, Milan, 2012.
13. J. Han, W. Zhang, T. Zhou, X. Wang and R. Xu, *RSC Adv.*, 2012, **2**, 8293.
14. H. N. Kagalwala, E. Gottlieb, G. Li, T. Li, R. Jin and S. Bernhard, *Inorg. Chem.*, 2013, **52**, 9094.
15. A. V. Malkov, A. J. P. Stewart-Liddon, F. Teplý, L. Kobr, K. W. Muir, D. Haigh and P. Kočovský, *Tetrahedron*, 2008, **64**, 4011.
16. P.-F. Teng, C.-S. Tsang, H.-L. Yeung, W.-L. Wong, W.-T. Wong and H.-L. Kwong, *J. Organomet. Chem.*, 2006, **691**, 5664.
17. D. Guo, C.-y. Duan, C.-j. Fang and Q.-j. Meng, *J. Chem. Soc., Dalton Trans.*, 2002, 834.
18. C. R. Rice, C. J. Baylies, L. P. Harding, J. C. Jeffery, R. L. Paul and M. D. Ward, *J. Chem. Soc., Dalton Trans.*, 2001, 3039.
19. A. M. Appel, D. H. Pool, M. O'Hagan, W. J. Shaw, J. Y. Yang, M. Rakowski DuBois, D. L. DuBois and R. M. Bullock, *ACS Catal.*, 2011, **1**, 777.
20. G. A. N. Felton, R. S. Glass, D. L. Lichtenberger and D. H. Evans, *Inorg. Chem.*, 2006, **45**, 9181.
21. A. J. Bard and L. R. Faulkner, *Electrochemical Methods: Fundamentals and Applications*, Wiley, New York, 2nd edn., 2001.
22. V. Artero and M. Fontecave, *Chem. Soc. Rev.*, 2013, **42**, 2338.
23. Y. Yamada, T. Miyahigashi, H. Kotani, K. Ohkubo and S. Fukuzumi, *Energy Environ. Sci.*, 2012, **5**, 6111.
24. C. Wang, S. Cao and W.-F. Fu, *Chem. Commun.*, 2013, **49**, 11251.

The pyridine-containing ligands **L1** and **L2** react with Ni^{2+} ions to afford dinuclear triple-stranded helicate and tetrahedral cage supramolecular complexes, respectively; the two architectures exhibit contrasting reactivity towards electro- and photocatalytic proton reduction.